Environmental Science & Technology

pubs.acs.org/est

Article

Simultaneous Sulfite Electrolysis and Hydrogen Production Using Ni Foam-Based Three-Dimensional Electrodes

Raúl A. Márquez-Montes, Kenta Kawashima, Kobe M. Vo, David Chávez-Flores, Virginia H. Collins-Martínez, C. Buddie Mullins, and Víctor H. Ramos-Sánchez*

Cite This: *Environ. Sci. Technol.* 2020, 54, 12511−12520

Read Online

ACCESS | Metrics & More | Article Recommendations | Supporting Information

ABSTRACT: The electrochemical oxidation of sulfite ions offers encouraging advantages for large-scale hydrogen production, while sulfur dioxide emissions can be effectively used to obtain value-added byproducts. Herein, the performance and stability during sulfite electrolysis under alkaline conditions are evaluated. Nickel foam (NF) substrates were functionalized as the anode and cathode through electrochemical deposition of palladium and chemical oxidation to carry out the sulfite electro-oxidation and hydrogen evolution reactions, respectively. A combined analytical approach in which a robust electrochemical flow cell was coupled to different *in situ* and *ex situ* measurements was successfully implemented to monitor the activity and stability during electrolysis. Overall, satisfactory sulfite conversion and hydrogen production efficiencies (>90%) at 10 mA·cm^{-2} were mainly attributed to the use of NF in three-dimensional electrodes with a large surface area and enhanced mass transfer. Furthermore, stabilization processes associated with electrochemical dissolution and sulfur crossover through the membrane induced specific changes in the chemical and physical properties of the electrodes after electrolysis. This study demonstrates that NF-based electrocatalysts can be incorporated in an efficient electrochemical flow cell system for sulfite electrolysis and hydrogen production, with potential applications at a large scale.

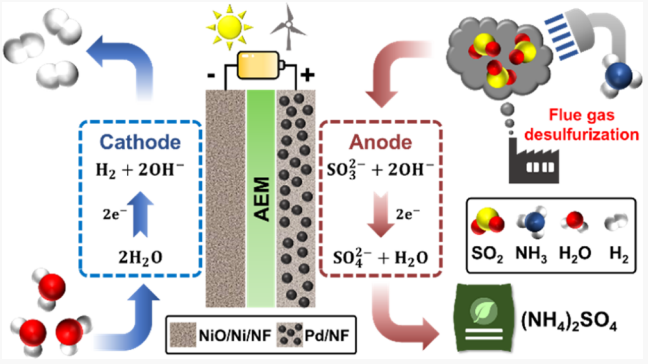

INTRODUCTION

Sulfur dioxide (SO_2) emissions produced from coal, heavy oil, and diesel combustion have led to severe effects on human health, climate change, and the global environment. East Asia is the most threatened region by anthropogenic SO_2 emissions because of China's high dependence on coal.[1,2] To mitigate the current situation, flue gas desulfurization (FGD) technologies have been implemented in order to capture SO_2 from gas streams in power plants.[3] In particular, wet-type technologies with high removal efficiencies are preferred, in which SO_2 becomes sulfite (SO_3^{2-}).[4,5] Then, by exposing the resulting solution to strong oxidants, such as ozone, disposals can be transformed into useful byproducts.[6] Notably, the use of aqueous ammonia as an absorbent with subsequent oxidation yields ammonium sulfate, which has potential use as a fertilizer.[7]

Electrochemical technologies have been extensively used for environmental remediation because of their exceptional removal efficiencies and superior performance.[8−11] Additionally, electrochemistry offers promising advantages for sustainable interconversion of chemical energy and electrical work because they can be supplied by green electrons from solar and wind power.[12] In the research field of FGD, recent studies have demonstrated that replacing typical chemical oxidation with electrochemical steps has great potential for harvesting profitable byproducts from disposals, thus lowering overall costs.[13−16] In particular, the electrochemical oxidation of ammonium sulfite at slightly alkaline pH yields high-purity hydrogen (H_2) and ammonium sulfate simultaneously, as recently demonstrated by our previous work.[13]

Figure 1 shows the ammonia-based FGD process, in which the oxidation step is performed *via* the electrochemical oxidation of sulfite. Extensive research has been done regarding the absorption step, including process simulation, scrubber design, and absorption models.[7,17−19] However, while absorption units and product handling technologies are commercially available,[20] the electrochemical step still leaves much to be improved and only preliminary studies and proofs of concept are available in the literature. Aspects such as sulfite speciation due to the pH,[13] the kinetics on Pd and Pt electrodes,[21,22] and preliminary hydrogen production measure-

Received: June 29, 2020
Revised: September 5, 2020
Accepted: September 9, 2020
Published: September 9, 2020

https://dx.doi.org/10.1021/acs.est.0c04190
Environ. Sci. Technol. 2020, 54, 12511−12520

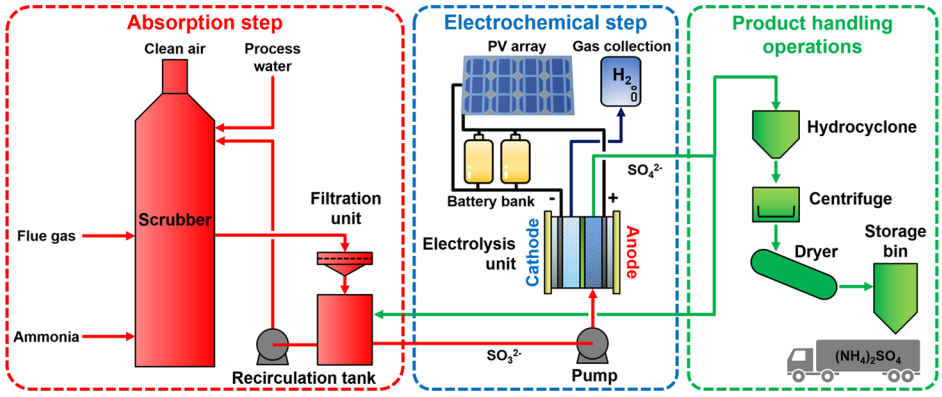

Figure 1. Schematic illustration of the ammonia-based FGD process with an electrochemical sulfite oxidation step.

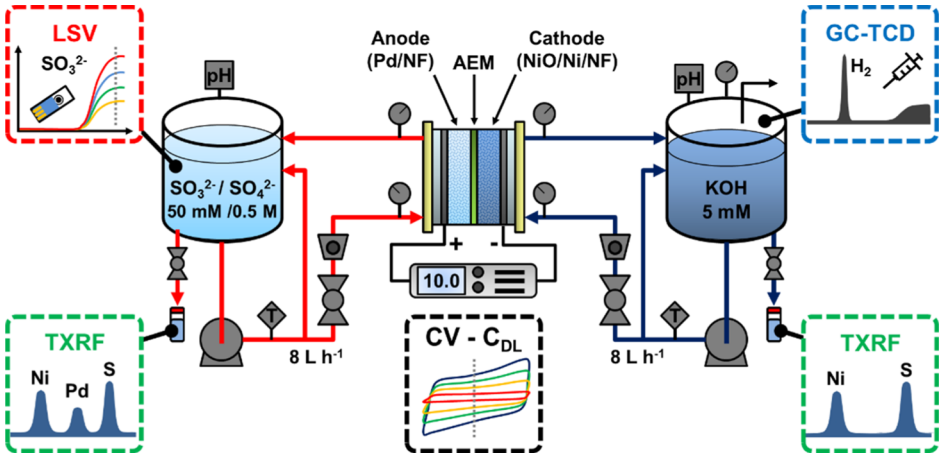

Figure 2. Schematic illustration of the flow cell system and the analytical techniques used to monitor electrolysis tests.

ments have been reported using typical three-electrode cells and planar electrodes.[13,23] Therefore, further improvement on electrode design, catalyst stability, and cell performance is required to improve the robustness of the step. In this sense, the use of nickel foam (NF) as a three-dimensional (3D) substrate for electrocatalysts offers promising advantages for novel technologies, as demonstrated in water electrolysis, because of its high conductivity, large surface area, and great stability in alkaline media.[24−26] Moreover, by depositing catalysts onto NF, costs can be effectively reduced, while mass transfer and the surface area are greatly improved.[27] In spite of these features, its use in electrochemical technologies for environmental applications is scarce and its potential in other approaches has not been fully tested.[28,29]

Herein, sulfite electrolysis using surface-modified NF electrodes in a novel electrochemical reactor design, as a pioneering electrochemical oxidation approach for FGD, is addressed. In brief, this article covers the performance and stability assessment of the electrodes during alkaline electrolysis in a robust electrochemical flow cell, which provides a more realistic and reproducible testing environment at the lab scale. Through a series of experiments, the performance in terms of H_2 production and SO_3^{2-} conversion as well as the physicochemical stability of the electrodes is discussed. This study is focused solely on the electrochemical step shown in Figure 1 because the remaining steps in FGD are well known and can be effectively adapted to specific flue gas compositions and flow rates. Still, the improvement of the electrochemical step offers important advantages, namely, (1) the production of high-purity H_2 and ammonium sulfate while SO_2 emissions are exploited, (2) the use of NF as an improved and cost-effective 3D substrate to increase the surface area of deposited electrocatalysts, and (3) the use of an easily scalable flow cell with superior performance. Further development should be aimed to successfully integrate this electrochemical step in FGD processes for validation at a large scale.

EXPERIMENTAL SECTION

Two different electrodes, namely, NiO/Ni/NF and Pd/NF, were fabricated. For comparison, bare NF and Pd/C/NF electrodes were also prepared and tested (Figure S1). NiO/Ni/NF electrodes were prepared by a simple chemical oxidation method using $K_2S_2O_8$ as previously reported by He *et al.*[30] Pd/NF electrodes were prepared by a one-step electrochemical plating method as previously reported by Wang *et al.*[31] A Pd loading of 0.49 ± 0.06 mg·cm^{-2} was obtained. The electrodes were characterized before and after electrolysis by X-ray diffraction (XRD), scanning electron microscopy (SEM), energy-dispersive X-ray spectroscopy (EDX), and X-ray photoelectron spectroscopy (XPS). The redox behavior and the electrochemically active surface area (ECSA) were estimated through electrochemical measurements. Details are given in the Supporting Information.

Sulfite electrolysis was performed during a 24 h period in a 3D-printed filter-press electrochemical flow cell as described in a previous work.[27] A schematic diagram of the one-unit flow cell system and the set of analytical techniques is shown in Figure 2. Electrodes were placed in each chamber (Figure S2):

https://dx.doi.org/10.1021/acs.est.0c04190
Environ. Sci. Technol. 2020, 54, 12511−12520

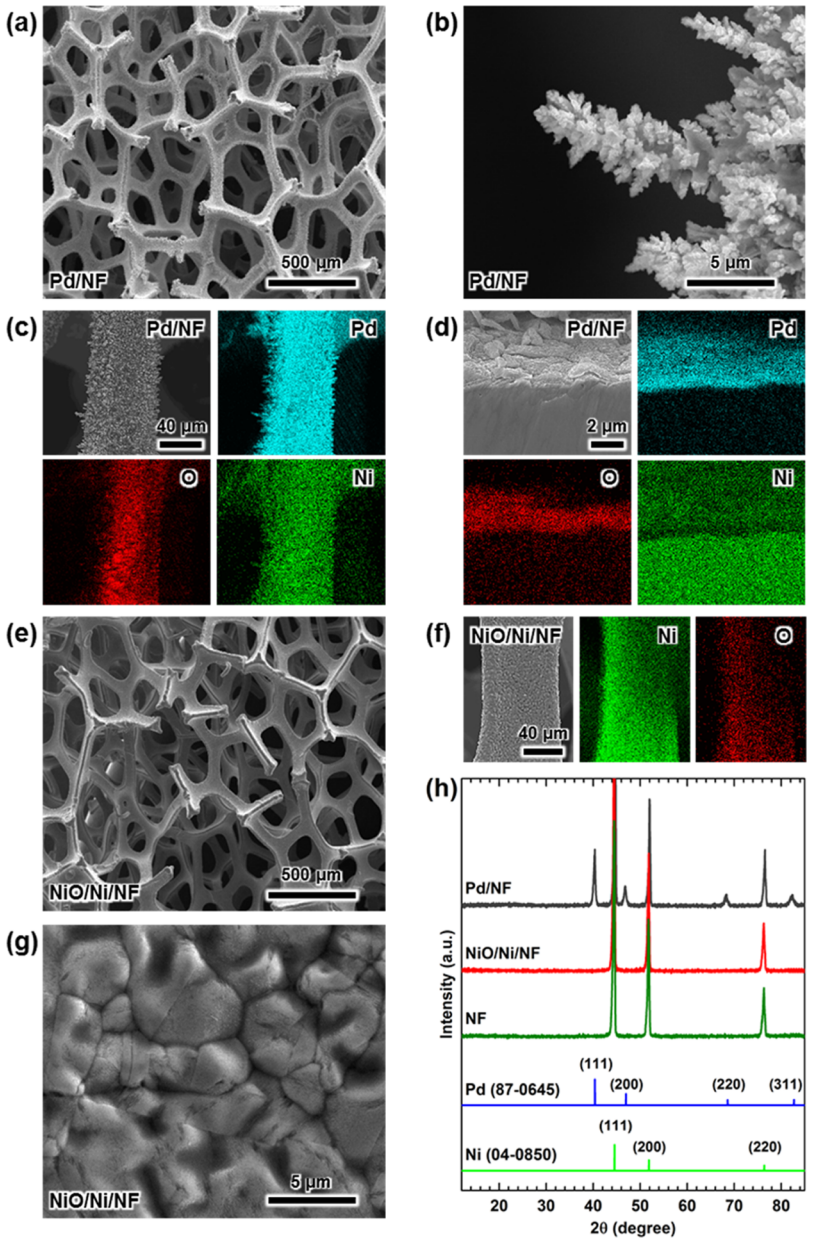

Figure 3. Electrode characterization: SEM images for the (a) Pd/NF porous network and (b) Pd dendrite, (c) elemental mapping for the Pd/NF branch, (d) elemental mapping for the Pd/NF cross section, (e) NiO/Ni/NF porous network, (f) elemental mapping for the NiO/Ni/NF branch, (g) NiO/Ni/NF surface, and (h) XRD results.

NiO/Ni/NF as the cathode and Pd/NF as the anode. Ni-coated stainless-steel plates were used as current collectors. A 5 mM KOH solution (pH ∼ 12) was recirculated in the cathodic section of the cell, while a fresh 50 mM $(NH_4)_2SO_3$ in 0.5 M $(NH_4)_2SO_4$ solution, as the supporting electrolyte, was loaded into the anodic section. The latter acted as a simulated electrolyte coming from a flue gas absorption step as used by previous studies.[5] For further details on the properties of the effluents from ammonia-based FGD, please refer Table S1 in the Supporting Information. A volume of 250 mL was used for each section. Importantly, KOH solutions were purified by using a previously reported method to remove Fe impurities to avoid incidental activity enhancement for the oxygen evolution reaction (OER) during tests.[32] Note that the anion exchange membrane (AEM) delimited both sections. The flow rate was maintained at 8 L h^{-1} using peristaltic pumps and calibrated rotameters. Electrolytes were degasified with ultrahigh purity Ar for 30 min before any tests.

Electrolysis was performed as chronopotentiometric runs at 10 mA·cm^{-2} using an Interface 1000 potentiostat/galvanostat (Gamry). Tests were carried out in a three-electrode configuration using an Ag/AgCl reference electrode. Anodic linear sweep voltammetry (LSV) scans between 0.0 and 1.3 V versus Ag/AgCl, at a scan rate of 10 mV·s^{-1}, were recorded before and after each test. For the cathode, LSV scans were recorded from −0.48 to −1.5 V versus Ag/AgCl at 10 mV·s^{-1}. All the potentials were converted into the reversible hydrogen electrode scale. The ECSA fluctuation along time was estimated by checking the double-layer capacitance (C_{DL}). Liquid samples (50 μL) were taken from the anolyte and analyzed to determine the sulfite concentration. The concentrations of Ni, Pd, and S in the electrolytes were

https://dx.doi.org/10.1021/acs.est.0c04190
Environ. Sci. Technol. 2020, 54, 12511−12520

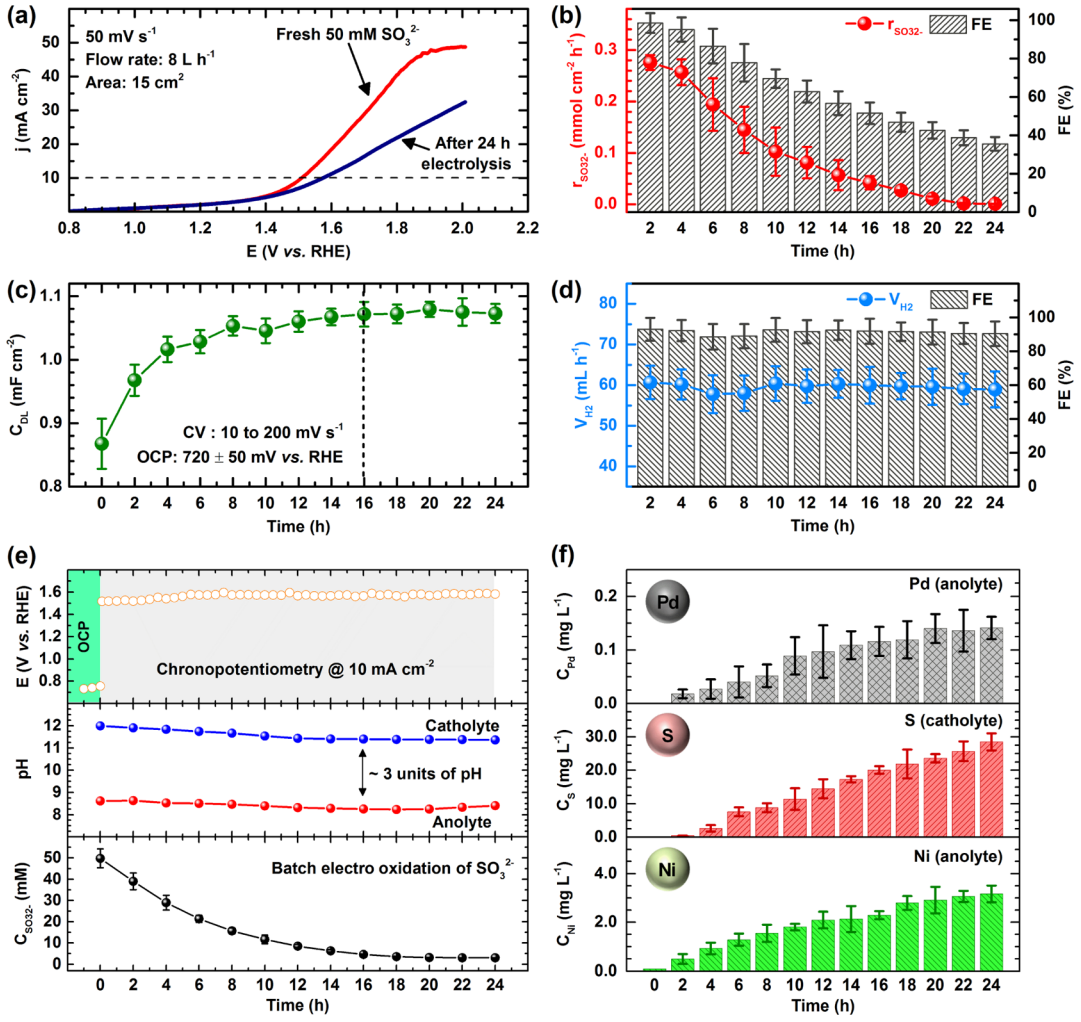

Figure 4. Electrolysis performance results: (a) anodic $i-V$ curves before and after electrolysis, (b) SO_3^{2-} consumption rates with the corresponding FEs, (c) double-layer capacitance of the anode with time, (d) H_2 production rates and the corresponding FEs, (e) electrode potential, pH, and SO_3^{2-} concentration with time, and (f) concentration of dissolved Pd, S, and Ni in the corresponding electrolytes with time.

assessed by means of total-reflectance X-ray fluorescence (TXRF). Samples were analyzed using an S2 PICOFOX spectrometer (Bruker Nano GmbH) by using an internal standard (Y, 5 mg L^{-1}). Finally, the evolved H_2 gas was estimated by means of gas chromatography. The faradaic efficiencies (FEs), reaction rates, and performance metrics were calculated. Details are given in the Supporting Information. Note: electrolysis tests were performed by triplicate.

RESULTS AND DISCUSSION

Electrode Characterization. SEM images of Pd/NF anodes are shown in Figures 3 and S4. For comparison, SEM and elemental mappings of pristine NF are shown in Figure S5. In both materials, interconnecting pores with diameters below 500 μm are distributed along a consistent 3D structure. However, while pristine NF exhibits a rather smooth surface, Pd/NF is covered with a dense layer of Pd microstructures. Remarkably, dendrite-like microstructures can be seen, especially near the edges of NF branches (Figure 3b). The diameter of the spikes protruding from these dendrites is estimated to be in the 50−500 nm range (Figure S4). Additional SEM images display Pd deposits deep within the porous substrate (Figure S6). Other tight spaces may not allow dendritic growth, which could explain Pd agglomeration (Figure S6a). EDX elemental mapping reveals that Pd uniformly covered the NF branches (Figure 3c), which demonstrates the high quality of Pd electrodeposition using a flow cell. A detailed analysis of a cross-sectional view of Pd/NF (Figure 3d) shows a thin Pd layer (~300 nm). The presence of oxygen on the surface is evident in EDX elemental mappings and atomic compositions (Table S2), suggesting that some Pd oxides could be formed by exposure to air. Still, only cubic Pd metal (ICDD PDF# 87-0645) and cubic Ni metal (ICDD PDF# 04-0850), which correspond to the as-deposited Pd and the NF substrate, respectively, can be seen in XRD patterns (Figure 3h).[31] Additionally, XPS measurements (Figure S9) confirmed the presence of Pd, Ni, and O. Overall, these results demonstrate that high-quality anodes were synthesized using a one-step electrodeposition method in a flow cell. The Pd electrocatalyst was distributed uniformly over the NF substrate and the observed dendrite-like morphology confers a large ECSA, which increases the number of exposed active sites for sulfite electro-oxidation. Therefore, superior Pd anodes can be obtained using a simple preparation method without requiring several synthetic steps.

For comparison, Pd/C/NF electrodes were prepared by spray coating. SEM images and elemental mapping are shown

https://dx.doi.org/10.1021/acs.est.0c04190
Environ. Sci. Technol. 2020, 54, 12511−12520

in Figure S8. In contrast to Pd/NF, the distribution of Pd is not homogeneous, and some portions of the NF substrate were exposed. Moreover, the catalyst severely agglomerates, creating flakelike microstructures which are stacked randomly. This suggests that Pd/C/NF electrodes prepared by spray coating are not useful because agglomeration decreases catalyst utilization, increases the inactive surface area (e.g., the carbon support and binder material), and ultimately results in a lower ECSA and higher cell resistance, as has been reported for Pt/C.[33,34] Therefore, binder-free Pd/NF anodes prepared by electrodeposition are a better alternative for sulfite electro-oxidation.

SEM images of the as-prepared NiO/Ni/NF cathodes are shown in Figures 3 and S9. Note that when compared with pristine NF (Figure S5), the NiO/Ni/NF electrode exhibits a slightly roughened surface which confers a larger surface area. This is more evident at the highest magnification (500 nm) as some nanostructures can be seen (Figure S9). Moreover, a significant presence of NiO nanoclusters was not evident, which suggests that the Ni surface was not substantially oxidized.[30] Although elemental mapping in Figure 3f shows both nickel and oxygen distributed along the NF branch, NiO peaks were not seen in the XRD patterns (Figure 3h), and only planes of the Ni metal are obvious. XPS analysis (Figure S10) showed only the presence of Ni, O, and C signals, which suggest that the NF surfaces of the as-obtained samples might be slightly oxidized.[30,35] This further demonstrates that only amorphous NiO clusters could be isolated over the cathode. Such an electrode composition favors the hydrogen evolution reaction (HER) because NiO promotes the cleavage of the H−OH bond, while contiguous metallic Ni preferentially adsorbs H, enhancing the overall recombination into H_2 and decreasing the overpotential.[30]

Additional electrochemical characterization was performed to compare the surface area and electrode activity. The ECSA was estimated through the C_{DL} method (Figure S11), while cyclic voltammetry (CV) was used to elucidate the redox behavior (Figure S12). Pd/NF displayed the highest ECSA, which is attributed to the dendrite-like microstructures produced by the well-controlled electrodeposition method. For NiO/Ni/NF, the noticeable improvement is attributed to an etching process *via* $K_2S_2O_8$ oxidation.[30] The removal of Ni roughened the surface, which may also improve bubble removal during the HER.[24] Regarding redox behavior, only Pd/NF and Pd/C/NF electrodes exhibited activity toward SO_3^{2-} electro-oxidation, while a higher HER activity is evident for NiO/Ni/NF compared to that for pristine NF. Indeed, this confirms the suitability of Pd/NF and NiO/Ni/NF electrodes for sulfite electro-oxidation and HER, respectively.

Performance and Stability Results. The sulfite electrolysis results are shown in Figure 4. From $i-V$ curves (Figure 4a), it is evident that SO_3^{2-} was fully consumed after 24 h. The initial curve exhibits an increase in the current density until it reaches the mass transfer-limited region close to 50 mA·cm^{-2}. After electrolysis, the curve no longer resembles that of SO_3^{2-} oxidation, and the potential at 10 mA·cm^{-2} shifts to ca. 80 mV. Figure 4b shows the sulfite electro-oxidation rates calculated from sulfite concentration profiles (Figure 4e) and the corresponding FEs. The electro-oxidation rates decrease with time since the availability of SO_3^{2-} dropped due to batch oxidation.[13] Moreover, the FEs are not constant and decrease as well. This implies that once SO_3^{2-} begins to be scarce in the electrolyte, simultaneous reactions proceeded because of a galvanostatic mode. It is evident that the secondary reaction which occurred at the anode is the OER because (1) bubble generation at the anode was observed especially after 6 h, (2) the $i-V$ curve after electrolysis closely resembles that of the OER, and (3) headspace samples from the anolyte container analyzed using a gas chromatograph and a thermal conductivity detector (TCD) demonstrate that evolved O_2 increased with time (Figure S13). Although this may appear to be unfavorable, we consider the OER to be beneficial because O_2 bubbles may enhance SO_3^{2-} oxidation in the bulk, in a similar way strong oxidants such as O_3 are bubbled in FGD disposals for the same purpose.[6] Furthermore, O_2 could be used as another byproduct in the overall process because the membrane avoids H_2 and O_2 from mixing.

As a benchmark, the performance of Pd/C/NF and NF electrodes was evaluated. The electro-oxidation rates were reduced notably after 8 h for Pd/C/NF (Figure S14), while pristine NF electrodes exhibited low FEs and $i-V$ curves resembling only OER activity (Figure S15). Evidently, pristine NF is not active toward SO_3^{2-} oxidation, as previously shown in the redox behavior characterization (Figure S12). The disadvantageous performance of the Pd/C/NF electrode is attributed to the reduced number of exposed Pd sites caused by catalyst agglomeration during spray coating, as previously described in the characterization section. Hence, even though both Pd/NF and Pd/C/NF electrodes had an equal catalyst loading, in the latter, less Pd active sites were in contact with sulfite ions. This further demonstrates the superior features of the Pd/NF anode.

An interesting behavior can be seen in Figure 4c, in which the C_{DL} at the anode stabilizes following an asymptotic trend. We attribute this behavior to a change in the ECSA as the reaction progresses, which implies that the initial surface condition may not be constant throughout electrolysis. Similar trends have been reported for OER electrocatalysts, in which the oxidation of the surface induced morphology and/or composition changes during OER.[36] In fact, this increase and stabilization of the ECSA throughout the OER has been previously seen.[37] This effect is discussed in detail in the following sections by comparing the electrodes before and after tests. Note that a similar effect was seen in bare NF (Figure S15), which can be attributed to Ni oxidation during the OER.[38]

The H_2 production rates and FEs are shown in Figure 4d. The hydrogen production rate was 0.252 ± 0.007 mmol h^{-1} cm^{-2} after averaging all the measurements during 20 h, which corresponds to approximately 60 mL of H_2 gas produced every 2 h using just one electrolysis unit. The FE was 91.3 ± 2.5% throughout electrolysis, and its fluctuation below 100% is attributed to the saturation of the electrolyte and bubbles attached to the walls of the catholyte container. Note that contrary to the anode, the FEs are constant because the HER is the dominant event. Overall, the results suggest that satisfactory FEs and H_2 production rates were achieved by more efficient bubble removal derived from the combination of NF and the flowing electrolyte, as compared to our previous work in a stagnant electrolyte and Pd foil electrode.[13] Furthermore, no other gas product was detected at the cathodic container, which proves that high-purity H_2 was produced during electrolysis and the AEM prevented O_2 migration from the anode.

Figure 4e shows that the electrode potential increases slightly with time. Still, this increment is only close to 8% of

https://dx.doi.org/10.1021/acs.est.0c04190
Environ. Sci. Technol. 2020, 54, 12511−12520

the initial potential, and it is associated to the OER occurring because of the depletion of the sulfite ion in the anode. Furthermore, a constant pH gradient is clearly seen between both sections, which is attributed to a constant flow of OH^- ions from the cathode to the anode.[13] Moreover, a constant ionic migration demonstrates an adequate stability of the membrane. The pH at the cathode fluctuated between 12 and 11.5, while at the anode, it was stable with a value around 8.5. These values of pH are advantageous for both electrodes, and severe basic conditions were effectively avoided. Sulfite electrooxidation is promoted above pH 8, while ammonia migration to the gas phase is decreased below pH 9.[21] Moreover, stable nickel oxides/hydroxides are expected in the pH range between 8.5 and 12.6 according to the Pourbaix diagram, which should decrease the dissolution rates of NF.[39] Finally, the sulfite concentration decreased with time, until it stabilized below 5 mM after 18 h. This validates the decrease of FEs and oxidation rates as the sulfite ion is depleted with time because of batch electrolysis.

Metal dissolution is caused by different factors such as electrode potential, pH, electrolyte composition, and surface oxidation/reduction, among others.[40−42] This unfavorable process may lead to a decrease in catalyst loading, which is detrimental to the performance and reaction rates with time.[42] Figure 4f shows the concentrations of Pd, S, and Ni in different electrolytes with time. We used the flow cell coupled to TXRF as a powerful approach to carefully measure the presence of elements in the electrolytes and assess electrode stability. For Pd and Ni, it is evident that some dissolution occurs at the anode. However, note that the metal concentration almost stabilizes after ca. 18 h. This implies that the dissolution rates decrease with time and are controlled. Metal dissolution in the Pd/C/NF electrode (Figure S14) was similar to that in Pd/NF, with a final Pd concentration close to 0.125 ± 0.087 mg·L^{-1}. Because both electrodes exhibited different ECSA trends, this suggests that Pd dissolution occurred until stabilization in the electrolyte and it was not related to the number of exposed Pd sites on each electrode. Moreover, the Ni-to-Pd ratio in the electrolyte was around 20:1, suggesting that the NF substrate was also etched until stabilization. Finally, the Ni concentration in the catholyte was low (<1 mg·L^{-1}) and stable, suggesting that the reductive potentials kept Ni as metallic.[39]

Sulfur detection at the cathode was used to estimate the sulfur diffusion through the membrane, a serious problem in SO_2 electrolyzers which reduces the efficiency at the cathode as S(IV) can be reduced to elemental sulfur or metallic sulfides.[43,44] From Figure 4f, note that the sulfur concentration at the cathode increases with time, which is attributed to the high concentration of sulfur at the anode and the high pressure drop due to porous NF, which may displace sulfite/sulfate ions through the AEM into the cathode.[27] Therefore, the effects on the cathode were evaluated. Figure 5 displays a series of electrochemical measurements to evaluate the activity and stability of the NiO/Ni/NF electrode. From Figure 5a, we observe that $i-V$ curves before and after electrolysis exhibit a similar HER behavior. The overpotential at 10 mA·cm^{-2} is ∼90 mV at the beginning and shifts near 20 mV. A similar trend can be seen from the chronopotentiometry curve (Figure 5b). Finally, ECSA fluctuation with time is subtle (Figure 5c), and a noticeable trend is not as evident as in Pd/NF (Figure 4c). This suggests that the electrode was stable and no serious poisoning due to S(IV) diffusion occurred. Still, post-analysis of the electrodes was performed to confirm these results.

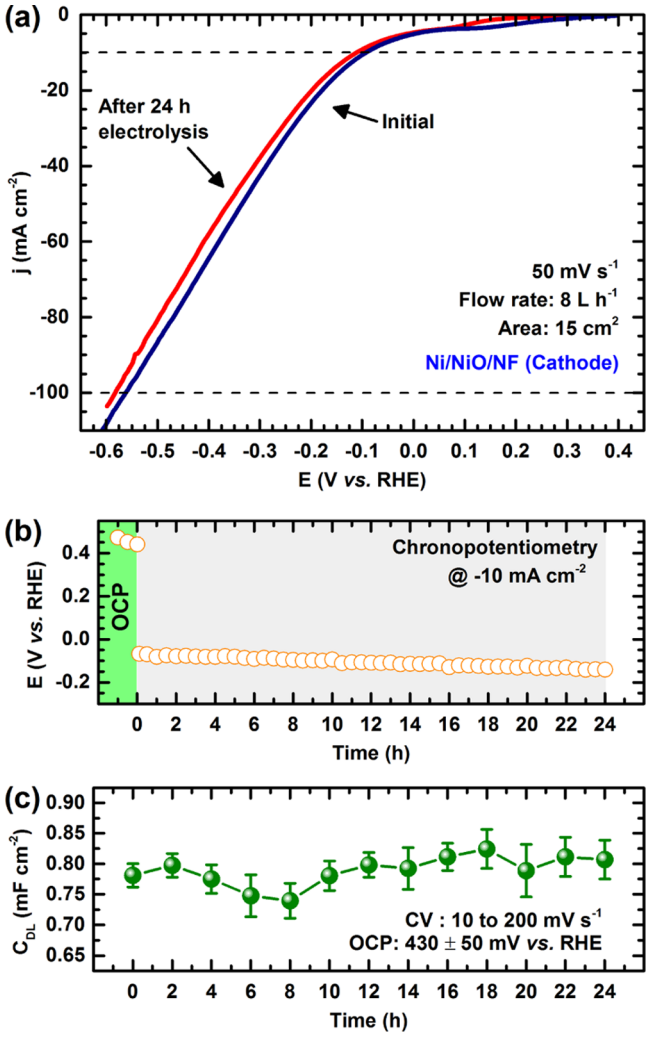

Figure 5. Electrochemical results for the NiO/Ni/NF cathode: (a) $i-V$ curves before and after electrolysis, (b) chronopotentiometric curve, and (c) double-layer capacitance with time.

Electrode Postanalysis. Figure S16 shows the morphology, EDX, and XRD comparisons before and after electrolysis using the Pd/NF anode. The cross section reveals a thick surface film (Figure S16a) mainly composed of Pd according to EDX (Figure S17). Dendrites exhibited a compressed, cauliflower-like structure as if sharp edges from the fresh electrode were removed (Figure S16b). This can be seen in more detail in additional SEM images (Figure S18). Overall, Pd deposits became rounded (Figure S16c), and higher magnifications (500 nm) revealed solid deposits (Figure S18) which are different from those in fresh Pd/NF (Figure S4). Also, Pd characteristic peaks from XRD were broadened (Figure S16f), which possibly indicates that the mean size of Pd crystallites was reduced.[45] Elemental mapping of the NF branches confirm that Pd was still dispersed uniformly throughout the material; however, the oxygen content was reduced (Figures S16d and S19). This is evident from EDX spectra, as the oxygen peak decreases (Figure S16e). This indicates that surface oxides were removed from the surface during electrolysis. Finally, note that no sulfur was detected, which suggests that the anode was not poisoned by the dithionate ion, a common anion which strongly adsorbs onto

https://dx.doi.org/10.1021/acs.est.0c04190
Environ. Sci. Technol. 2020, 54, 12511−12520

noble metals during sulfite electro-oxidation.[21,46] This further confirms the superior features of the Pd/NF electrode.

The results suggest that Pd electrodissolution occurred and surface oxides were removed until a stable condition was achieved: (i) the ECSA increased with time until it was constant; (ii) the Pd concentration in the electrolyte increased until it was stabilized according to TXRF; (iii) oxygen on the surface from EDX was decreased; and (iv) morphological changes suggest that sharp edges and spikes in Pd microstructures were removed. According to the literature, the anodic dissolution of Pd causes surface morphology changes, and oxide growth/reduction leads to an increase of surface defects.[40] Furthermore, Pd oxide transitions (e.g., from PdO to PdO_2) trigger dissolution in alkaline media.[47] Nevertheless, note that the Pd/NF anode still exhibited a high surface area, Pd was well dispersed after electrolysis, and dissolution was not severe. In fact, it has been found that Pd exhibits lower anodic dissolution rates than most noble metals in alkaline media.[47] This is attributed to the stabilization provided by adsorbed OH^-.[40] Therefore, it is likely that initial Pd surface oxides were etched until fresh metallic Pd was exposed. In contrast, anodic Ni dissolution is attributed to pH because soluble Ni^{2+} is expected below pH ~ 8.3.[39] Therefore, pH control is crucial. Still, it seems that only small amounts of exposed Ni were dissolved, as shown by EDX (Figure 5e) and a stable Ni concentration after 20 h (Figure 3f).

SEM, EDX, and XRD measurements of the NiO/Ni/NF electrode are shown in Figure S20. The morphology remained unchanged (Figure S21): a rough surface with nanostructures is evident. This agrees with the constant ECSA trend (Figure 4c). From XRD, we observe that characteristic peaks of metallic Ni remained unchanged. However, elemental mappings and EDX spectra revealed that the oxygen and sulfur contents increased after electrolysis (Figure S21b,c and Table S2). We performed XPS analysis to elucidate the chemical states of Ni, O, and S (Figure S22). The surface was mainly composed of Ni metal, NiO, and $Ni(OH)_2$. The presence of reduced Ni is discussed in the Supporting Information. Peaks typical of a metal−sulfur bond in the range of 160.5−163.8 eV were not seen, which suggests that SO_4^{2-} ions arising from sulfur diffusion were not reduced and only adsorption occurs.[48−50] This further confirms the robustness of the NiO/Ni/NF electrode; the efficiency was not decreased because of sulfur reduction, and the HER is the main reaction, which agrees with FEs.

Performance, Energy, and Environmental Implications. The performance metrics and relevant operational parameters are shown in Table 1. Our approach exhibited reasonable performance at 10 $mA{\cdot}cm^{-2}$ with high SO_3^{2-} conversions (>90%) and a constant H_2 production rate (~0.25 mmol h^{-1} cm^{-2}). Considering the energy inputs and outputs, a rough energy efficiency can be estimated. One electrolysis unit requires about 0.11 $kW{\cdot}h{\cdot}mol^{-1}$ H_2 produced, while the energy output as hydrogen can be set as 0.08 $kW{\cdot}h{\cdot}mol^{-1}$ (see the Supporting Information).[51] Thus, the energy efficiency of the electrolyzer is about 73%. When pumping is considered, the efficiency drops drastically (<5%). The use of a membrane also contributes to a higher cell voltage (~2.0 V). Note however that these features improve the overall performance: AEM-separated streams allow a safe way to collect gas and liquid products,[52] while forced convection and recirculation enhance bubble removal, ion migration, and mass transfer.[27,53,54] Future studies should be aimed to reduce energy consumption, and energy assessments should consider the entire FGD process because pumping is also required for fluid transportation.

Table 1. Performance Metrics for the SO_3^{2-} Electrolysis Approach Proposed Here

H_2 productivity ($mmol{\cdot}cm^{-2}{\cdot}h^{-1}$)	0.252 ± 0.007[c]
H_2 productivity ($mmol{\cdot}cm^{-3}{\cdot}h^{-1}$)	0.015 ± 0.001[c]
H_2 purity (%)	32.0 ± 1.2[a,c]
H_2 average FE (%)	91.3 ± 2.5[c]
initial SO_3^{2-} oxidation rate ($mmol{\cdot}cm^{-2}{\cdot}h^{-1}$)	0.276 ± 0.014[b]
initial SO_3^{2-} oxidation rate ($mmol{\cdot}cm^{-3}{\cdot}h^{-1}$)	0.017 ± 0.001[b]
final SO_3^{2-} concentration (mM)	1.96 ± 0.79[b]
SO_3^{2-} conversion (%)	96.8 ± 1.6[b]
cell voltage (V)	2.03 ± 0.12
energy yield ($mol{\cdot}kW{\cdot}h^{-1}$)	9.19 ± 0.58
energy consumption ($kW{\cdot}h{\cdot}mol^{-1}$)	0.11 ± 0.01

[a]Remaining gases were Ar and H_2O. No other gas was produced at the cathode. [b]Value from averaging different electrolysis tests. [c]Value from averaging measurements for 20 h.

Most of the approaches in the literature only oxidize sulfite and lack the profitable by-products proposed herein. Studies focused only on SO_2 removal reported higher conversions. An ozonation method assisted by Mn^{2+} achieved almost a 99% conversion,[6] while gas/solid oxidation on MnO_2 reached nearly 100%.[55] However, a fair comparison is difficult because configurations were not strictly the same. Furthermore, some electrochemical systems with simultaneous SO_3^{2-} oxidation and H_2 production have been reported. The photo-electrochemical system reported by Han *et al.*, which relied on Pt (cathode) and Mo-doped $BiVO_4$ (photoanode), reported similar conversions (~97%) and FEs (94%) but lower H_2 production rates (<60.26 $\mu mol{\cdot}cm^{-2}{\cdot}h^{-1}$) at 3.42 $mA{\cdot}cm^{-2}$.[14] Huang reported a H_2 production of 3.63 $mmol{\cdot}cm^{-2}{\cdot}h^{-1}$ with Pt/C electrodes (0.5 $mg{\cdot}cm^{-2}$). However, large current densities (~180 $mA{\cdot}cm^{-2}$) and a concentrated ammonium sulfite electrolyte (2 M) were required.[23] A method reported by Yang *et al.*, which allowed the recovery of H_2SO_4, NaOH, and H_2 in a parallel-plate reactor, exhibited a lower FE (~87%) and a higher energy consumption (~0.2 $kW{\cdot}h{\cdot}mol^{-1}$ H_2) when operating at a low current density (5.92 $mA{\cdot}cm^{-2}$) and a higher cell voltage (3.6 V).[16] Finally, the use of a flow cell and forced convection greatly improved H_2 production from our previous approach (0.05 $mmol{\cdot}cm^{-2}{\cdot}h^{-1}$).[13]

Besides performance, other important technical aspects should be highlighted. First, the use of a 3D-printed electrolyzer proves that 3D printing may accelerate electrolysis with a reduction in costs and weight.[56] Pilot plant-scale electrolyzers with stacked units using 3D-printed components should be assessed because of the unique advantages of 3D printing for scale-up.[27] Additionally, coupling the system to high-efficiency triple-junction solar cells is highly recommended as it has been previously used to increase solar-to-hydrogen efficiencies in polymer electrolyte membrane (PEM) electrolyzers.[57,58] Moreover, note that extra purification steps are required, especially when flue gas contains other chemicals, such as heavy metals. For instance, filtration using membranes or molecular sieves can be used. Furthermore, hydrocyclones and centrifuges coupled to recirculation steps are required to concentrate and purify resultant product streams and subsequently generate solid ammonium sulfate. These purification technologies are commercially available.[20]

https://dx.doi.org/10.1021/acs.est.0c04190
Environ. Sci. Technol. 2020, 54, 12511−12520

Furthermore, this approach carries important environmental and sustainability implications. First, note that the atom economy of the process is greatly improved. That is, more atoms involved in the process are included in the final products, *i.e.*, ammonium sulfate and hydrogen. Typical FGD is mostly focused on SO_2 removal from flue gas to satisfy environmental regulations. However, by making this process more profitable, environmental treatment of flue gas may become a ubiquitous process. Also, ammonia-based FGD requires fewer and easier steps than analogous processes such as limestone-based FGD, which requires more complex unit operations after the oxidation step.[20] Additionally, by using an electrochemical step and aqueous electrolytes, the use of homogeneous catalysts, solvents, ionic liquids, and ozone for oxidation is avoided. Still, some issues must be effectively solved to enhance the approach. In particular, long-term electrode stability and metal dissolution must be carefully addressed because Pd and Ni toxicity may become an issue, especially if the oxidized solution is discharged in water after FGD.[59] Of course, microfiltration systems could be employed to capture dissolved metals for reuse.[60] Other aspects such as the use of greener materials for 3D printing, research on earth-abundant electrocatalysts for sulfite electro-oxidation and HER, AEM development, and coupling to renewable energy sources should be assessed to increase the sustainability of the approach. Ultimately, this may lead to profitable, efficient, and environmentally friendly SO_2 exploitation technologies capable of being integrated into coal-fired power plants in the future.

■ ASSOCIATED CONTENT

Supporting Information

The Supporting Information is available free of charge at https://pubs.acs.org/doi/10.1021/acs.est.0c04190.

Detailed experimental section, additional electrochemical and physicochemical characterization results before and after experiments, electrochemical testing setup, oxygen evolution plots with time, and additional post-analysis results (PDF)

■ AUTHOR INFORMATION

Corresponding Author

Víctor H. Ramos-Sánchez − *Facultad de Ciencias Químicas, Universidad Autónoma de Chihuahua, Chihuahua, Chihuahua 31125, Mexico; Department of Mechanical and Aerospace Engineering, University of California San Diego, La Jolla, California 92093, United States;* orcid.org/0000-0001-8030-0393; Email: vramos@uach.mx, vramossanchez@ucsd.edu

Authors

Raúl A. Márquez-Montes − *Facultad de Ciencias Químicas, Universidad Autónoma de Chihuahua, Chihuahua, Chihuahua 31125, Mexico;* orcid.org/0000-0003-3885-5007

Kenta Kawashima − *Department of Chemistry, The University of Texas at Austin, Austin, Texas 78712, United States;* orcid.org/0000-0001-7318-6115

Kobe M. Vo − *McKetta Department of Chemical Engineering, The University of Texas at Austin, Austin, Texas 78712, United States;* orcid.org/0000-0002-7680-1627

David Chávez-Flores − *Facultad de Ciencias Químicas, Universidad Autónoma de Chihuahua, Chihuahua, Chihuahua 31125, Mexico;* orcid.org/0000-0001-6852-0406

Virginia H. Collins-Martínez − *Centro de Investigación en Materiales Avanzados, Chihuahua, Chihuahua 31136, Mexico*

C. Buddie Mullins − *Department of Chemistry, McKetta Department of Chemical Engineering, and McKetta Department of Chemical Engineering, Texas Materials Institute, and Center for Electrochemistry, The University of Texas at Austin, Austin, Texas 78712, United States;* orcid.org/0000-0003-1030-4801

Complete contact information is available at: https://pubs.acs.org/10.1021/acs.est.0c04190

Author Contributions

The manuscript was written through contributions of all authors. All authors have given approval to the final version of the manuscript.

Notes

The authors declare no competing financial interest.

■ ACKNOWLEDGMENTS

R.A.M.M. (CVU 919871) wishes to thank CONACYT for his master's scholarship award as well as the Mexican Ministry of Foreign Relations (SRE) and the Consulate of Mexico in Austin for the Matías Romero Visiting Scholars Program. V.H.R.S. (CVU 163636) recognizes the financial support from CONACYT for his sabbatical stay in the University of California, San Diego. K.K., K.M.V., and C.B.M. also gratefully acknowledge the National Science Foundation (NSF) *via* grant CHE-1664941 for support of the analytical portion of this work and the Welch Foundation through grant F-1436 for their generous support. The authors would like to thank Dr. Hugo Celio for his assistance in XPS measurements. Discussions and comments on experiments to prepare the Fe-free KOH aqueous solution with Yoon Jun Son are thankfully acknowledged.

■ ABBREVIATIONS

NF	Ni foam
Pd/C	Pd on carbon
Pd/NF	Pd electrodeposited onto Ni foam
Pd/C/NF	Pd/C spray-coated onto Ni foam

■ REFERENCES

(1) Yan, S.; Wu, G. SO2 Emissions in China—Their Network and Hierarchical Structures. *Sci. Rep.* **2017**, *7*, 46216.

(2) Su, S.; Li, B.; Cui, S.; Tao, S. Sulfur Dioxide Emissions from Combustion in China: From 1990 to 2007. *Environ. Sci. Technol.* **2011**, *45*, 8403−8410.

(3) Xu, Y.; Williams, R. H.; Socolow, R. H. China's Rapid Deployment of SO2 Scrubbers. *Energy Environ. Sci.* **2009**, *2*, 459−465.

(4) Xu, Y. China's Functioning Market for Sulfur Dioxide Scrubbing Technologies. *Environ. Sci. Technol.* **2011**, *45*, 9161−9167.

(5) Huang, C.; Linkous, C. A.; Adebiyi, O.; T-Raissi, A. Hydrogen Production via Photolytic Oxidation of Aqueous Sodium Sulfite Solutions. *Environ. Sci. Technol.* **2010**, *44*, 5283−5288.

(6) Nie, M.-Y.; Gu, C.; Zhong, K.-L.; Fang, Y.-J. Catalytic Oxidation Removal of Sulfur Dioxide by Ozone in the Presence of Metallic Ions. *Energy Fuels* **2012**, *26*, 5590−5595.

(7) Gao, X.; Ding, H.; Du, Z.; Wu, Z.; Fang, M.; Luo, Z.; Cen, K. Gas−Liquid Absorption Reaction between (NH4)2SO3 Solution and SO2 for Ammonia-Based Wet Flue Gas Desulfurization. *Appl. Energy* **2010**, *87*, 2647−2651.

(8) Qian, A.; Yuan, S.; Zhang, P.; Tong, M. A New Mechanism in Electrochemical Process for Arsenic Oxidation: Production of H2O2 from Anodic O2 Reduction on the Cathode under Automatically

Developed Alkaline Conditions. *Environ. Sci. Technol.* **2015**, *49*, 5689−5696.
(9) Muthuraman, G.; Moon, I. S. Sustainable Generation of a Homogeneous Ni(I) Catalyst in the Cathodic Compartment of a Divided Flow Electrolytic Cell for the Degradation of Gaseous Carbon Tetrachloride by Electroscrubbing. *ACS Sustainable Chem. Eng.* **2016**, *4*, 1364−1372.
(10) Lei, Y.; Remmers, J. C.; Saakes, M.; van der Weijden, R. D.; Buisman, C. J. N. Influence of Cell Configuration and Long-Term Operation on Electrochemical Phosphorus Recovery from Domestic Wastewater. *ACS Sustainable Chem. Eng.* **2019**, *7*, 7362−7368.
(11) Guo, Q.; Sun, T.; Wang, Y.; He, Y.; Jia, J. Spray Absorption and Electrochemical Reduction of Nitrogen Oxides from Flue Gas. *Environ. Sci. Technol.* **2013**, *47*, 9514−9522.
(12) Pereira, E. C.; Cuesta, A. A Personal Perspective on the Role of Electrochemical Science and Technology in Solving the Challenges Faced by Modern Societies. *J. Electroanal. Chem.* **2016**, *780*, 355−359.
(13) Márquez-Montes, R. A.; Orozco-Mena, R. E.; Camacho-Dávila, A. A.; Pérez-Vega, S.; Collins-Martínez, V. H.; Ramos-Sánchez, V. H. Optimization of the Electrooxidation of Aqueous Ammonium Sulfite for Hydrogen Production at Near-Neutral PH Using Response Surface Methodology. *Int. J. Hydrogen Energy* **2020**, *45*, 13821−13831.
(14) Han, J.; Cheng, H.; Zhang, L.; Fu, H.; Chen, J. Trash to Treasure: Use Flue Gas SO2 to Produce H2 via a Photo-electrochemical Process. *Chem. Eng. J.* **2018**, *335*, 231−235.
(15) Dourado, A. H. B.; Munhos, R. L.; Silva, N. A.; Colle, V. D.; Carvalho, G. G. A.; Oliveira, P. V.; Arenz, M.; Varela, H.; Córdoba de Torresi, S. I. Opportunities and Knowledge Gaps of SO2 Electro-catalytic Oxidation for H2 Electrochemical Generation. *ACS Catal.* **2019**, *9*, 8136−8143.
(16) Yang, C.; Hu, Y.; Cao, L.; Yang, J. Circulating Regeneration and Resource Recovery of Flue Gas Desulfurization Residuals Using a Membrane Electroreactor: From Lab Concept to Commercial Scale. *Environ. Sci. Technol.* **2012**, *46*, 11273−11279.
(17) Jia, Y.; Yin, L.; Xu, Y.; Ding, X.; Sheng, G. A Model for Performance of Sulfite Oxidation of Ammonia-Based Flue Gas Desulfurization System. *Atmos. Pollut. Res.* **2015**, *6*, 997−1003.
(18) Asif, M.; Kim, W.-S. Modeling and Simulation of the Combined Removal of SO2 and CO2 by Aqueous Ammonia. *Greenhouse Gases: Sci. Technol.* **2014**, *4*, 509−527.
(19) Jia, Y.; Zhong, Q.; Fan, X.; Wang, X. Kinetics of Oxidation of Total Sulfite in the Ammonia-Based Wet Flue Gas Desulfurization Process. *Chem. Eng. J.* **2010**, *164*, 132−138.
(20) Lu, P.; McLinden, D.Ammonia-Based Flue Gas Desulfurization. *Power Eng.* 2017, *121*, (7) https://www.power-eng.com/2017/07/12/ammonia-based-flue-gas-desulfurization/.
(21) Márquez-Montes, R. A.; Orozco-Mena, R. E.; Lardizábal-Gutiérrez, D.; Chávez-Flores, D.; López-Ortíz, A.; Ramos-Sánchez, V. H. Sulfur Dioxide Exploitation by Electrochemical Oxidation of Sulfite in Near-Neutral PH Electrolytes: A Kinetics and Mechanistic Study. *Electrochem. Commun.* **2019**, *104*, 106481.
(22) Skavås, E.; Hemmingsen, T. Kinetics and Mechanism of Sulphite Oxidation on a Rotating Platinum Disc Electrode in an Alkaline Solution. *Electrochim. Acta* **2007**, *52*, 3510−3517.
(23) Huang, C. Solar Hydrogen Production via Pulse Electrolysis of Aqueous Ammonium Sulfite Solution. *Sol. Energy* **2013**, *91*, 394−401.
(24) Chaudhari, N. K.; Jin, H.; Kim, B.; Lee, K. Nanostructured Materials on 3D Nickel Foam as Electrocatalysts for Water Splitting. *Nanoscale* **2017**, *9*, 12231−12247.
(25) Grdeń, M.; Alsabet, M.; Jerkiewicz, G. Surface Science and Electrochemical Analysis of Nickel Foams. *ACS Appl. Mater. Interfaces* **2012**, *4*, 3012−3021.
(26) van Drunen, J.; Pilapil, B. K.; Makonnen, Y.; Beauchemin, D.; Gates, B. D.; Jerkiewicz, G. Electrochemically Active Nickel Foams as Support Materials for Nanoscopic Platinum Electrocatalysts. *ACS Appl. Mater. Interfaces* **2014**, *6*, 12046−12061.
(27) Márquez-Montes, R. A.; Collins-Martínez, V. H.; Pérez-Reyes, I.; Chávez-Flores, D.; Graeve, O. A.; Ramos-Sánchez, V. H. Electrochemical Engineering Assessment of a Novel 3D-Printed Filter-Press Electrochemical Reactor for Multipurpose Laboratory Applications. *ACS Sustainable Chem. Eng.* **2020**, *8*, 3896−3905.
(28) Kartikaningsih, D.; Huang, Y.-H.; Shih, Y.-J. Electro-Oxidation and Characterization of Nickel Foam Electrode for Removing Boron. *Chemosphere* **2017**, *166*, 184−191.
(29) Zhu, Y.; Qiu, S.; Deng, F.; Ma, F.; Li, G.; Zheng, Y. Three-Dimensional Nickel Foam Electrode for Efficient Electro-Fenton in a Novel Reactor. *Environ. Technol.* **2020**, *41*, 730−740.
(30) He, B.; Kuang, Y.; Hou, Z.; Zhou, M.; Chen, X. Enhanced Electrocatalytic Hydrogen Evolution Activity of Nickel Foam by Low-Temperature-Oxidation. *J. Mater. Res.* **2017**, *33*, 213−224.
(31) Wang, N.; Tao, B.; Miao, F.; Zang, Y. Electrodeposited Pd/Graphene/ZnO/Nickel Foam Electrode for the Hydrogen Evolution Reaction. *RSC Adv.* **2019**, *9*, 33814−33822.
(32) Trotochaud, L.; Young, S. L.; Ranney, J. K.; Boettcher, S. W. Nickel−Iron Oxyhydroxide Oxygen-Evolution Electrocatalysts: The Role of Intentional and Incidental Iron Incorporation. *J. Am. Chem. Soc.* **2014**, *136*, 6744−6753.
(33) Lee, S.-K.; Kim, C.-H.; Cho, W.-C.; Kang, K.-S.; Park, C.-S.; Bae, K.-K. The Effect of Pt Loading Amount on SO2 Oxidation Reaction in an SO2-Depolarized Electrolyzer Used in the Hybrid Sulfur (HyS) Process. *Int. J. Hydrogen Energy* **2009**, *34*, 4701−4707.
(34) Carmo, M.; Doubek, G.; Sekol, R. C.; Linardi, M.; Taylor, A. D. Development and Electrochemical Studies of Membrane Electrode Assemblies for Polymer Electrolyte Alkaline Fuel Cells Using FAA Membrane and Ionomer. *J. Power Sources* **2013**, *230*, 169−175.
(35) Li, C.; Hou, J.; Wu, Z.; Guo, K.; Wang, D.; Zhai, T.; Li, H. Acid Promoted Ni/NiO Monolithic Electrode for Overall Water Splitting in Alkaline Medium. *Sci. China Mater.* **2017**, *60*, 918−928.
(36) Wygant, B. R.; Kawashima, K.; Mullins, C. B. Catalyst or Precatalyst? The Effect of Oxidation on Transition Metal Carbide, Pnictide, and Chalcogenide Oxygen Evolution Catalysts. *ACS Energy Lett.* **2018**, *3*, 2956−2966.
(37) Kim, J.-H.; Kawashima, K.; Wygant, B. R.; Mabayoje, O.; Liu, Y.; Wang, J. H.; Mullins, C. B. Transformation of a Cobalt Carbide (Co3C) Oxygen Evolution Precatalyst. *ACS Appl. Energy Mater.* **2018**, *1*, 5145−5150.
(38) Doyle, R. L.; Godwin, I. J.; Brandon, M. P.; Lyons, M. E. G. Redox and Electrochemical Water Splitting Catalytic Properties of Hydrated Metal Oxide Modified Electrodes. *Phys. Chem. Chem. Phys.* **2013**, *15*, 13737−13783.
(39) Huang, L.-F.; Hutchison, M. J.; Santucci, R. J.; Scully, J. R.; Rondinelli, J. M. Improved Electrochemical Phase Diagrams from Theory and Experiment: The Ni−Water System and Its Complex Compounds. *J. Phys. Chem. C* **2017**, *121*, 9782−9789.
(40) Grdeń, M.; Łukaszewski, M.; Jerkiewicz, G.; Czerwiński, A. Electrochemical Behaviour of Palladium Electrode: Oxidation, Electrodissolution and Ionic Adsorption. *Electrochim. Acta* **2008**, *53*, 7583−7598.
(41) Cherevko, S.; Zeradjanin, A. R.; Topalov, A. A.; Kulyk, N.; Katsounaros, I.; Mayrhofer, K. J. J. Dissolution of Noble Metals during Oxygen Evolution in Acidic Media. *ChemCatChem* **2014**, *6*, 2219−2223.
(42) Jovanovič, P.; Hodnik, N.; Ruiz-Zepeda, F.; Arčon, I.; Jozinović, B.; Zorko, M.; Bele, M.; Šala, M.; Šelih, V. S.; Hočevar, S.; Gaberščček, M. Electrochemical Dissolution of Iridium and Iridium Oxide Particles in Acidic Media: Transmission Electron Microscopy, Electrochemical Flow Cell Coupled to Inductively Coupled Plasma Mass Spectrometry, and X-Ray Absorption Spectroscopy Study. *J. Am. Chem. Soc.* **2017**, *139*, 12837−12846.
(43) Gasik, M. M.; Virtanen, J.; Santasalo-Aarnio, A. Improved Operation of SO2 Depolarized Electrolyser Stack for H2 Production at Ambient Conditions. *Int. J. Hydrogen Energy* **2017**, *42*, 13407−13414.
(44) Santasalo-Aarnio, A.; Virtanen, J.; Gasik, M. SO2 Carry-over and Sulphur Formation in a SO2-Depolarized Electrolyser. *J. Solid State Electrochem.* **2016**, *20*, 1655−1663.

https://dx.doi.org/10.1021/acs.est.0c04190
Environ. Sci. Technol. 2020, 54, 12511−12520

(45) Uvarov, V.; Popov, I. An Estimation of the Correctness of XRD Results Obtained from the Analysis of Materials with Bimodal Crystallite Size Distribution. *CrystEngComm* **2015**, *17*, 8300−8306.
(46) Gasana, E.; Westbroek, P.; Temmerman, E.; Thun, H. P. Electrochemical Behaviour of Sodium Dithionite at a Platinum Electrode and Determination of Diffusion Coefficient in Alkaline Solution. *Anal. Commun.* **1999**, *36*, 387−389.
(47) Schalenbach, M.; Kasian, O.; Ledendecker, M.; Speck, F. D.; Mingers, A. M.; Mayrhofer, K. J. J.; Cherevko, S. The Electrochemical Dissolution of Noble Metals in Alkaline Media. *Electrocatalysis* **2018**, *9*, 153−161.
(48) Ou, X.; Luo, Z. One-Step Synthesis of Ni3S2 Nanoplatelets on Graphene for High Performance Supercapacitors. *RSC Adv.* **2016**, *6*, 10280−10284.
(49) Ganesan, P.; Sivanantham, A.; Shanmugam, S. Inexpensive Electrochemical Synthesis of Nickel Iron Sulphides on Nickel Foam: Super Active and Ultra-Durable Electrocatalysts for Alkaline Electrolyte Membrane Water Electrolysis. *J. Mater. Chem. A* **2016**, *4*, 16394−16402.
(50) Sivanantham, A.; Ganesan, P.; Shanmugam, S. Hierarchical NiCo2S4 Nanowire Arrays Supported on Ni Foam: An Efficient and Durable Bifunctional Electrocatalyst for Oxygen and Hydrogen Evolution Reactions. *Adv. Funct. Mater.* **2016**, *26*, 4661−4672.
(51) Joshi, A. S.; Dincer, I.; Reddy, B. V. Effects of Various Parameters on Energy and Exergy Efficiencies of a Solar Thermal Hydrogen Production System. *Int. J. Hydrogen Energy* **2016**, *41*, 7997−8007.
(52) Singh, M. R.; Papadantonakis, K.; Xiang, C.; Lewis, N. S. An Electrochemical Engineering Assessment of the Operational Conditions and Constraints for Solar-Driven Water-Splitting Systems at near-Neutral PH. *Energy Environ. Sci.* **2015**, *8*, 2760−2767.
(53) Modestino, M. A.; Walczak, K. A.; Berger, A.; Evans, C. M.; Haussener, S.; Koval, C.; Newman, J. S.; Ager, J. W.; Segalman, R. A. Robust Production of Purified H2 in a Stable, Self-Regulating, and Continuously Operating Solar Fuel Generator. *Energy Environ. Sci.* **2014**, *7*, 297−301.
(54) Modestino, M. A.; Hashemi, S. M. H.; Haussener, S. Mass Transport Aspects of Electrochemical Solar-Hydrogen Generation. *Energy Environ. Sci.* **2016**, *9*, 1533−1551.
(55) Wu, H.; Cai, W.; Long, M.; Wang, H.; Wang, Z.; Chen, C.; Hu, X.; Yu, X. Sulfur Dioxide Capture by Heterogeneous Oxidation on Hydroxylated Manganese Dioxide. *Environ. Sci. Technol.* **2016**, *50*, 5809−5816.
(56) Chisholm, G.; Kitson, P. J.; Kirkaldy, N. D.; Bloor, L. G.; Cronin, L. 3D Printed Flow Plates for the Electrolysis of Water: An Economic and Adaptable Approach to Device Manufacture. *Energy Environ. Sci.* **2014**, *7*, 3026−3032.
(57) Jia, J.; Seitz, L. C.; Benck, J. D.; Huo, Y.; Chen, Y.; Ng, J. W.; Bilir, T.; Harris, J. S.; Jaramillo, T. F. Solar Water Splitting by Photovoltaic-Electrolysis with a Solar-to-Hydrogen Efficiency over 30%. *Nat. Commun.* **2016**, *7*, 13237.
(58) Jacobsson, T. J.; Fjällström, V.; Edoff, M.; Edvinsson, T. Sustainable Solar Hydrogen Production: From Photoelectrochemical Cells to PV-Electrolyzers and Back Again. *Energy Environ. Sci.* **2014**, *7*, 2056−2070.
(59) Ispas, C.; Andreescu, D.; Patel, A.; Goia, D. V.; Andreescu, S.; Wallace, K. N. Toxicity and Developmental Defects of Different Sizes and Shape Nickel Nanoparticles in Zebrafish. *Environ. Sci. Technol.* **2009**, *43*, 6349−6356.
(60) Aydiner, C.; Bayramoglu, M.; Keskinler, B.; Ince, O. Nickel Removal from Waters Using a Surfactant-Enhanced Hybrid Powdered Activated Carbon/Microfiltration Process. II. The Influence of Process Variables. *Ind. Eng. Chem. Res.* **2009**, *48*, 903−913.

https://dx.doi.org/10.1021/acs.est.0c04190
Environ. Sci. Technol. 2020, 54, 12511−12520